Wear 462–463 (2020) 203512

Contents lists available at ScienceDirect

Wear

journal homepage: http://www.elsevier.com/locate/wear

Tribological behaviour of galvanic gold coatings reinforced with silica nanoparticles

G. Heymans, A. Igual Muñoz *, S. Mischler

Ecole Polytechnique Fédérale de Lausanne, Tribology and Interface Chemistry Group, EPFL SCI STI SM, Station 12, CH-1015 Lausanne, Switzerland

ARTICLE INFO

Keywords:
Gold
Nanoparticles
Galvanic coatings
Composite coatings
Friction
Silica

ABSTRACT

Electroplated composite Au/SiO_2 coatings on a nickel substrate have been produced by dispersing an emulsion of silica nanoparticles (20 nm in diameter) in an industrial hard-gold bath. The tribological behaviour of the Au/SiO_2 coatings with different SiO_2 content were investigated under sliding conditions against an alumina counterpart at different loads and sliding velocities. The tribological induced transformation of the coated surfaces were analysed using 3D-profilometry, scanning electron microscopy (SEM), focused-ion beam (FIB) cross sectioning and Auger electron spectroscopy (AES). The composite coatings provide higher hardness and ten-fold longer lubricating lifetime compared to the original hard gold coating. Hardness was identified as a key factor reducing the adhesive component of friction and increasing the resistance of gold against smearing. These effects allow to postpone the exposure of the nickel substrate and thus the loss of the self-lubricating character of the coating.

1. Introduction

Gold is a precious transition metal which is well known to have unique physical and chemical properties that make this material attractive for different industrial applications (jewelry, electronics or microtechnique). Among those properties, good chemical stability, high electrical conductivity and good ductility and malleability can be highlighted [1–3]. In particular, electroplated gold is commonly used in electronics and in micromechanical systems as solid lubricant coatings [4–7]. Indeed, thanks to its malleability, gold accommodates large frictional stresses without wearing. However gold coated surfaces lose their lubricating properties once the substrate material is exposed to the contacting surfaces [8–10]. More in detail, the wear mechanisms of electroplated gold coatings proposed by several authors [8,10–12] involve different stages including thinning of the coating by ploughing the gold until the underlying substrate appears on the surface, subsurface deformation and generation of wear particles. More specifically, the first wear mechanism proposed by Tian et al. for fretting conditions [8] for electroplated gold coating on a brass material with a nickel intermediate layer includes a first stage in which gold was pushed out making the underlying nickel appearing in the contact, a second one in which cracks were initiated and propagated with potential generation of wear particles from the nickel-brass interface and a final stage in which accumulation of oxides in the contact took place. Those different stages were monitored by the transitions in friction which changed from low to high values. These multilayer systems were also studied by Bayer's group [9,11] who included a wear mechanism considering sub-surface deformation (including buckling of the nickel layer) as the main cause of wear in connector systems.

Clearly, in order to increase the lifetime of self-lubricating gold coated surfaces, it appears convenient to increase their resistance against deformation and smearing. This can be achieved by incorporating a second phase (ceramic, carbon fibres, polymers) into the metallic matrix. Indeed, electrochemical codeposition of nanoparticles with different metals, such as Ni, NiFe or Cu, but not Au, in order to improve the tribological performance of the resulting coatings was already reported [13,14]. Incorporation of hard ceramic particles (i.e. Al_2O_3, SiO_2 or SiC) into nickel galvanic coatings was found to increase their microhardness [15,16]. Moreover, Song et al. could increase the lifetime of gold coated electrical contacts by the addition of hard metal oxide nanoparticles (TiO_2 and Al_2O_3) [17]. This paper does not investigate the wear phenomenon nor the frictional behaviour of the tested materials. The reason why ceramic nanoparticles improved lifetime remains unclear.

This work was initiated with the aim to better understand the mechanism by which nanoparticles incorporated into a gold coating

* Corresponding author.
E-mail address: anna.igualmunoz@epfl.ch (A.I. Muñoz).

https://doi.org/10.1016/j.wear.2020.203512
Received 18 May 2020; Received in revised form 12 September 2020; Accepted 8 October 2020
Available online 10 October 2020

affect its tribological properties. For this, electrochemical codeposition of hard gold from a bath containing monodispersed SiO_2 nanoparticles was carried out. The obtained coatings were evaluated under sliding conditions against an alumina counterpart using a laboratory tribometer. The investigated surfaces were characterized in terms of wear and frictional mechanisms.

2. Materials and methods

2.1. Materials and reagents

Pure nickel (99.9%) rod 12 mm in diameter was used as substrate for Au electrochemical deposition. An acidic hard gold solution with 2 g/L of gold in form of $KAu(CN)_2$ and 0.35 g/L of Nickel and pH 4.3 was used for producing the galvanic coatings tests.

Aqueous emulsion containing 30% wt of SiO_2 nanoparticles, 20 nm in diameter and pH 10 were used. The SiO_2 nanoparticles were dispersed in the Au bath by ultrasound sonication in order to generate a stable suspension with two different SiO_2 concentrations: 0.48 and 2.4 %vol.

2.2. Electrochemical codeposition

Galvanostatic depositions of Au and Au–SiO_2 suspensions were carried out at an applied constant current density of -1.7 mA/cm^2 during 2250 s using a rotating disk electrode at 100 rpm. Temperature of the electrolytic baths was kept constant at 30 °C. A three electrode electrochemical cell was used for the galvanic depositions with the nickel electrode disk, an exposed area of 1.13 cm^2 as a working electrode, a platinum wire as counter-electrode and a saturated calomel electrode reference (0.196 V vs SHE). An Autolab PGSTAT30 potentiostat was used for carrying out the electrochemical tests.

Microhardness of the resulting coatings was measured by a Vickers microhardness tester (Leitz) applying a normal load of 0.981 N during 15 s in three different locations.

2.3. Tribological tests

The tribological tests were carried out in a ball-on-disk configuration using an Al_2O_3 counterpart 6 mm in diameter, with a reciprocating motion of 3 mm wear track length, frequency of 2 Hz (sliding speed of 12 mm/s), normal load of 2.8 N and 20.000 cycles. In order to analyse the influence of sliding frequency and normal load, some tribological tests were also carried out at 5 Hz (sliding speed of 30 mm/s) and 5 N respectively. The normal and frictional load were continuously monitored so that the evolution of the coefficient of friction as a function of time was obtained.

Two replicas of all tests under the same conditions were carried out in order to check for the reproducibility of the data.

2.4. Surface characterization

A laser scanning confocal microscope (Keyance VK-X250) and 3D white light interferometer (GBS smartWLI) were used to quantify the material loss caused by wear and for characterizing the surface topography of the worn and unworn areas. Wear morphology was analysed by scanning electron microscope (SEM Phillips XLF30) and energy dispersive x-ray spectrometer (EDS). Subsurface deformations were checked by carrying out cross-sections in the wear tracks perpendicular to the sliding direction through a focus-ion-beam (FIB) and high-resolution field emission SEM (Zeiss XB540), milling the surface with a Ga + ion beam.

Nanoindentation measurements were carried out inside and outside of the wear tracks with a nanoindenter (Anton Paar) by applying an increasing loading up to 2 mN at 25 mN/min with a Berkovich diamond tip.

After the tribological tests, surface analysis inside of the wear tracks was carried out by Auger electron spectroscopy (AES) in a PHI 680 Scanning Auger Nanoprobe (Physical Electronics GmbH, Germany) using tilted angle of 30° and an energy of 10 keV (5 nA) electron-beam. Depth profile acquisition was done by scanning at 2 keV (1 μA) Ar + beam over an area of 1 × 1 mm^2. The sputter rate of SiO_2 standards measured under those conditions was 20 nm/min.

3. Results

3.1. Composite coating characterization

During the galvanic deposition of Au, the measured potential lied around −1035 mV, while in the Au/SiO_2 emulsions, the measured potential was slightly lower and the scatter slightly higher. The small differences are due to the presence of non-conductive particles in the electrolytic bath.

Morphology of the obtained coatings was studied by microscopic techniques. Fig. 1 shows an example of a SEM image and a FIB cross-section of the Au and the Au-0.48SiO2 coatings. Typical globular growth of the gold coating is shown in Fig. 1a and the homogenous growth of the gold and composite coating with an average thickness of 1.2 μm is shown in Fig. 1b and c respectively.

The EDX analysis of the composite coatings allowed to determine their SiO_2 content, resulting in a concentration of 8 %vol and 9 %vol in the Au-0.48SiO2 and Au-2.4SiO2 respectively. The fact that two different bath concentrations yield a similar incorporation rate is not surprising. Indeed, it was shown that the incorporation rate increases with the particle concentration in the bath till a critical particle concentration is reached above which the incorporation rate remains constant [18]. As expected, the microhardness of those composite coatings increases with increasing SiO_2 content, and also 9% increase in hardness from the Au-0.48SiO2 to the Au-2.4SiO2 is found as shown in Table 1. This confirms the hardening effect of the incorporation of SiO_2 nanoparticles in the gold matrix.

In Table 1, the microhardness of the substrate is also summarized together with the microhardness, nanohardness, elastic modulus (E) and surface roughness (Sa, given in nm) of the different coatings. Interestingly there is an opposite trend in hardness evolution with silica content depending on the micro and nano hardness measurement. Indeed, the silica incorporation leads to a decrease in nanohardness but to a larger microhardness. This opposite trend can be linked to the depth of indentation that in case of nanohardness is confined at the outermost surface of the gold layer (0.14 μm) while in the microhardness it goes deep into the substrate (4 μm penetration). Moreover, the indentation width in the nanohardness measurement corresponds to 1 μm, i.e. the same size of the columns in the gold coating (Fig. 1) while in the microindentation the width is much larger (30 μm) and comprises more than 60 gold columns and 30 nickel grains (Fig. 1).

3.2. Coefficient of friction

Fig. 2 shows the evolution of the coefficient of friction of the Ni, the Au and Au–SiO_2 coatings when sliding against an alumina ball at 2 Hz and at an applied normal load of 2.8 N. COF of Ni is shown in Fig. 2 as reference and it remained constant around a value of 0.3 during the whole test, showing a slight trend towards higher values with time. The Au coating reduces the COF of the system to a value around 0.2 for the first 2000 cycles, after which the COF starts increasing and reaches values above 0.3 before 4.000 cycles. In the case of the Au–SiO_2 composite coatings with 0.48 and 2.4 %vol SiO_2, the COF is slightly lower than the Au one, remaining around 0.15 during the whole test.

The average values of COF of Ni and other coatings are summarized in Table 2. Two different values of COF are shown in the table, corresponding to two independent tests carried out in two different samples under the same experimental conditions.

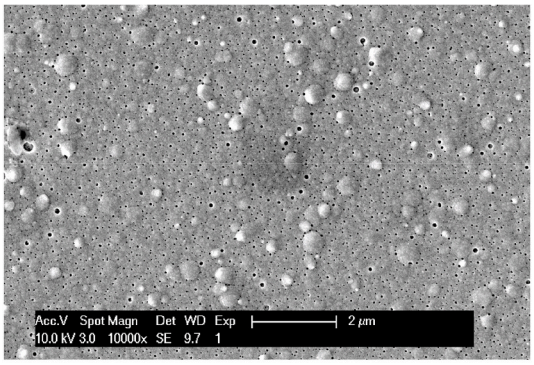

(a)

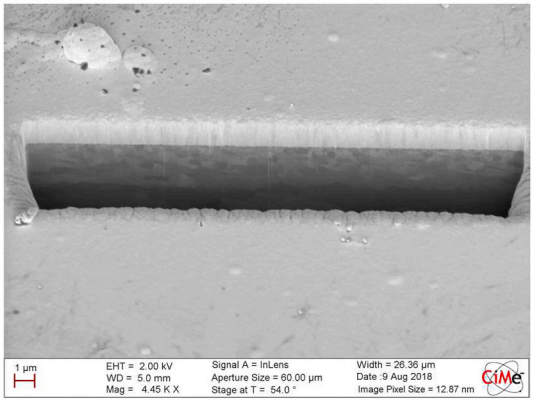

(b)

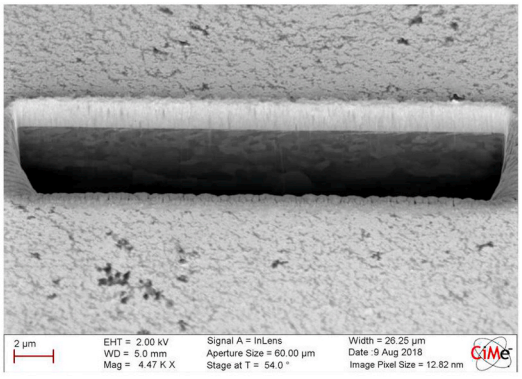

(c)

Fig. 1. SEM images of (a) Au coating, (b) Au coating FIB cross-section and (c) Au-0.48SiO2 FIB cross-section.

3.3. Morphological and topographical characterization of the worn surfaces

Typical optical (left) and white light interferometry (right) images of the Au and different Au–SiO_2 wear tracks obtained at the end of the tribological tests are shown in Fig. 3. In them, the central part of the wear track is shown. Very rough and dark areas were obtained in the Au coating, while much smoother areas with the shape of the ball counterpart are shown by the composite coatings with 0.48 %vol and 2.4 % vol SiO_2. In those cases, the gold coating still remained in the contact and only in some of the scratches, the underlying nickel appeared.

Table 1
Average potential value during the galvanostatic deposition, microhardness, nanohardness, elastic modulus (E) and surface roughness (Sa) values of the nickel substrate and the different gold and composite coatings.

	Ni	Au	Au-0.48SiO2	Au-2.4SiO2
Potential (mV)		−1035 ± 0.2	−1050 ± 15	−1040 ± 4
Microhardness (HV)	108 ± 6	106 ± 3	132 ± 1	144 ± 7
Nanohardness (HV)	327 ± 72	245 ± 11	209 ± 5	150 ± 7
E (GPa)	182 ± 40	126 ± 17	114 ± 4	101 ± 11
Surface roughness (Sa in nm)	20 ± 2	17 ± 8	26 ± 6	22 ± 4

Table 2
Average coefficient of friction (COF) of Ni, Au, Au-0.48SiO2 and Au-2.4SiO2. The values recorded during two independent tests are shown.

Sample	Load (N)	Frequency (Hz)	COF
Ni	2.8	2	0.34
			0.31
Au	2.8	2	0.31
			0.30
		5	0.26
			0.24
	5	5	0.25
Au-0.48 SiO2	2.8	2	0.18
			0.16
		5	0.14
			0.13
	5	5	0.12
Au-2.4 SiO2	2.8	2	0.16
			0.16
		5	0.1
			0.1

Typical SEM images of the wear tracks after the wear tests carried out on the Ni disks coated with Au and Au-0.48SiO2 are shown in Fig. 4a and b, respectively. The worn area in the Au coating shows a heavily damaged appearance with the Au plastically deformed and the Ni from the substrate coming out. Cracks are also visible at the surface. In the case of the Au-0.48SiO2 coating, some scratches are visible along the sliding direction but most of the worn surface is still covered by a plastically deformed Au layer.

The alumina ball counterpart was also analysed at the end of the wear tests. Fig. 5 shows the corresponding confocal images of the alumina ball after being rubbed for 20.000 cycles against the Au coating, Fig. 5a and the Au-0.48SiO2 composite coating, Fig. 5b. Scratches and damaged areas with some Au traces are clearly visible on the alumina after sliding against the Au coating. On the contrary, when the alumina ball was rubbed against the Au-0.48SiO2 coating, the ball does not show damaged areas, only some yellow patches corresponding to Au transfer can be observed.

3.4. Subsurface morphology: FIB cross-section of the worn areas

Subsurface deformation of the coatings was analysed by carrying out FIB cross-sections in the wear tracks. Fig. 6a shows an example of a FIB cross-section in the wear track of the Au coating at the end of the wear test sliding against an alumina ball during 20.000 cycles at 2 Hz and normal load of 2.8 N. In the image, a heavily deformed Ni substrate is covered by a non-uniformed layer of Au coming from the smeared coating. A mix layer of Au, Ni and of Al from the counterpart was also found in top-local sites of the contact. The subsurface morphology of the Au-0.48SiO2 coating after the same wear test is shown in Fig. 6b. In this case, the same deformation of the nickel substrate can be observed, although the extent of the coating damage is less pronounced. Only

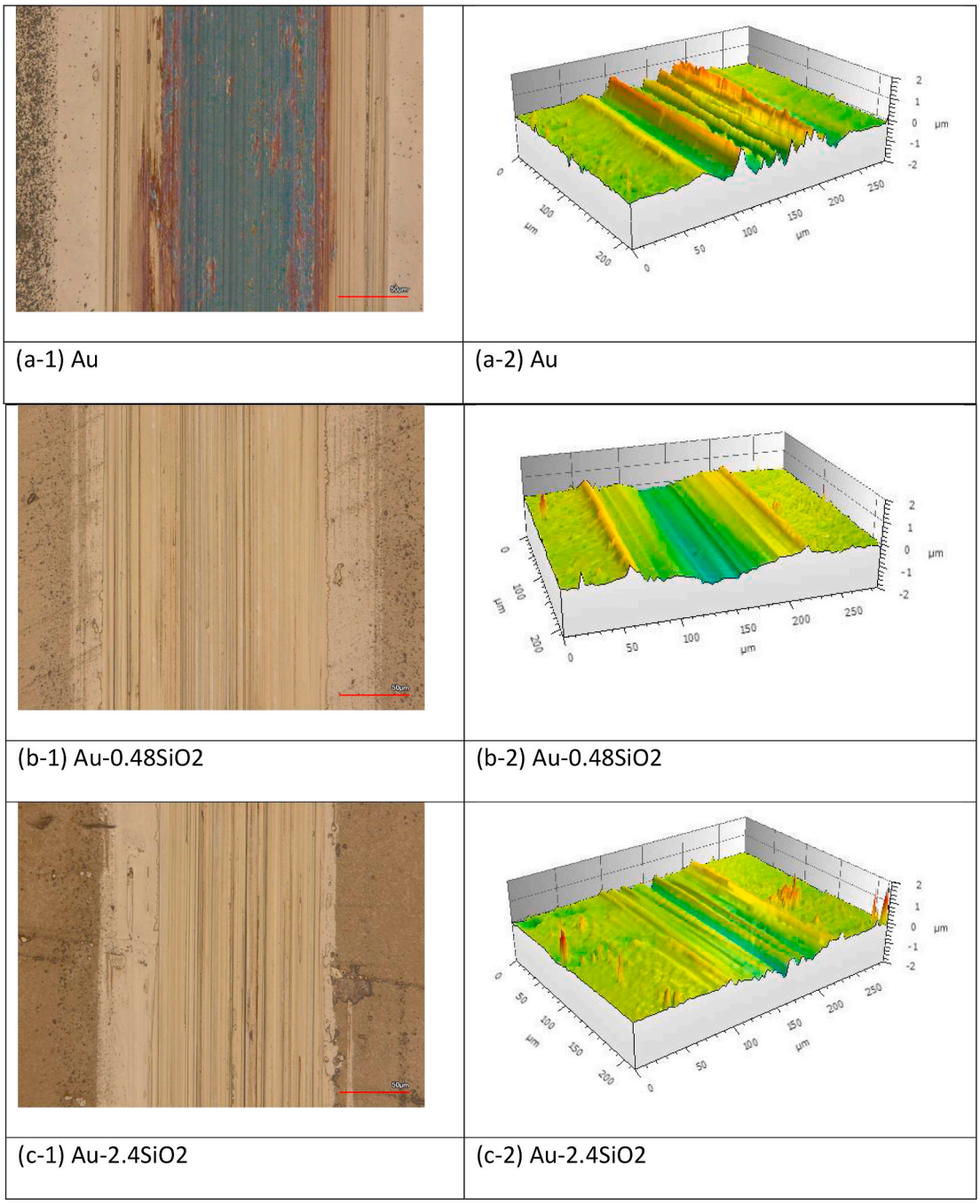

Fig. 3. Optical (left) and 3D images (right) of the wear track on the disk from (a) Au, (b) Au-0.48SiO2 and (c) Au-2.4SiO2 after sliding against an alumina counterpart during 20.000 cycles at 2 Hz and 2.8 N.

localized rupture of the coating was observed in which Ni exposure takes place and contacted the counterpart (black zones in Fig. 6b).

3.5. Surface chemistry of the worn areas

AES was carried out in the vicinity of the FIB cross-section in order to check the chemical composition of the worn areas. Fig. 7a shows the SEM image of the FIB-cross section in the wear track of the Au coating and the four points in which the AES profiles were measured. Except point 1, in which still some Au from the original coating was remaining, in the other locations, a mixture oxide of nickel (from the substrate) and aluminium (from the alumina counterpart) was formed. Fig. 7b and c shows two AES profiles of points 1 and 2 indicated in the SEM image (Fig. 7a).

Analogously, the chemical analysis of the wear track in the Au-0.48SiO2 coating is shown in Fig. 8. It is possible to observe how the main part of the wear track is still covered with the composite coating, Fig. 8b (point 1 in the SEM image) and that only in localized areas such as point 3, the nickel from the substrate exposes to the contact, Fig. 8c. The appearance of nickel is followed by an increase in the oxygen signal meaning that oxidized nickel is present in the wear track.

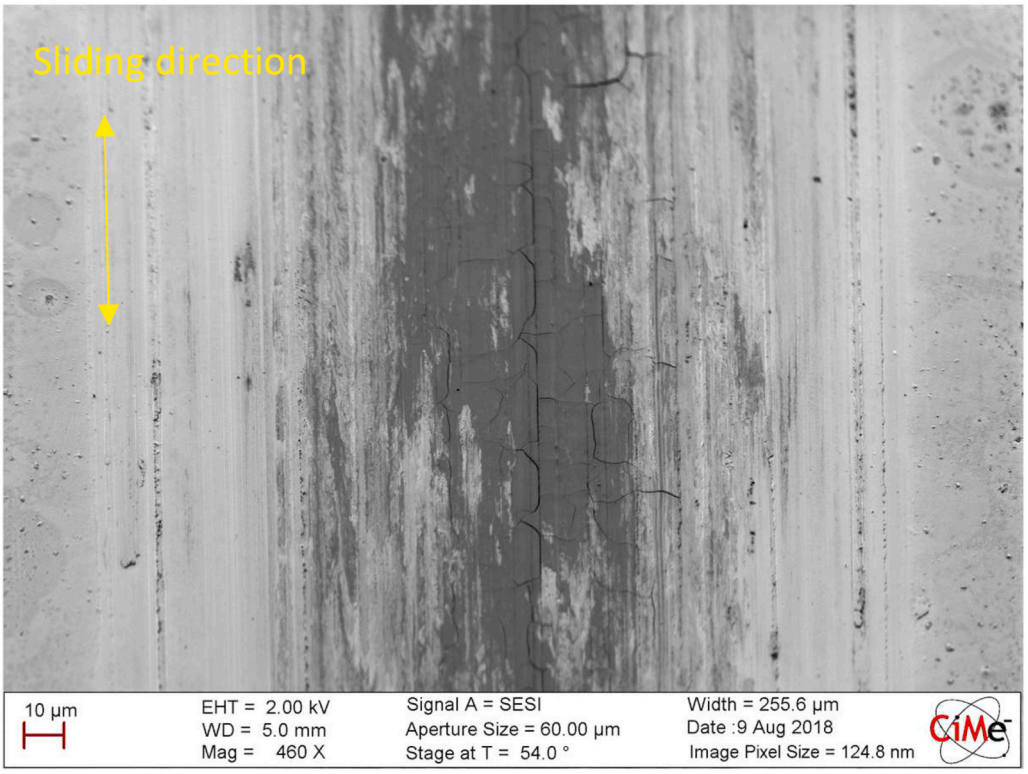

(a)

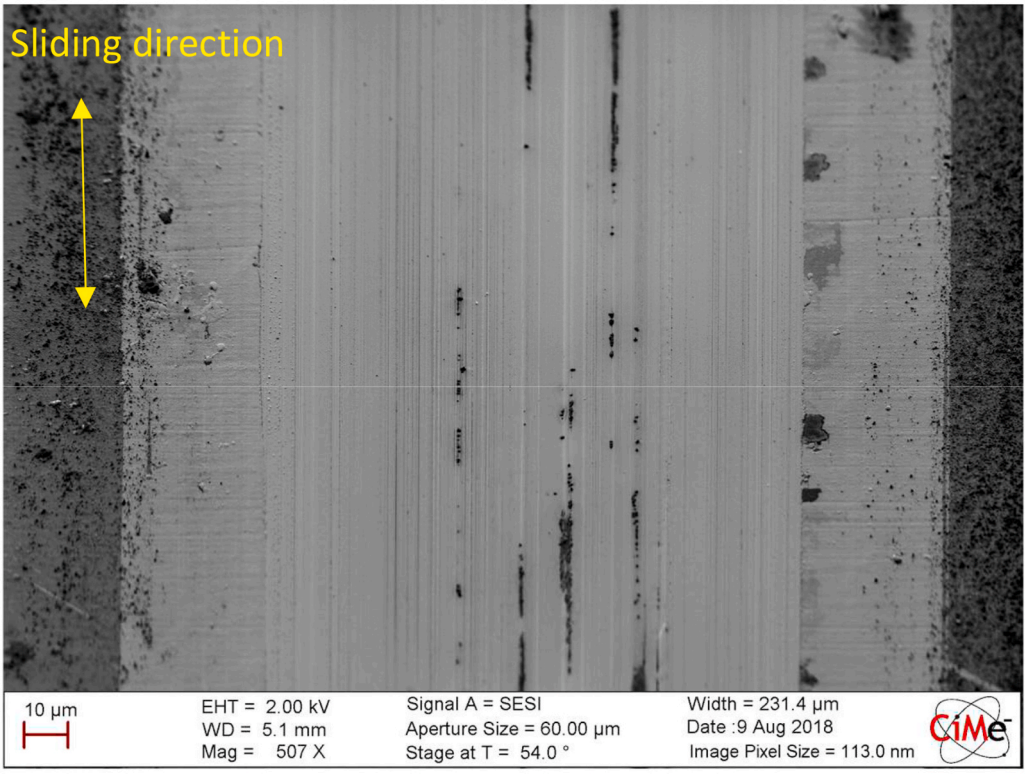

(b)

Fig. 4. SEM images of the wear track on (a) Au and (b) Au–048SiO2 coatings after sliding against an alumina counterpart during 20.000 cycles at 2 Hz and 2.8 N.

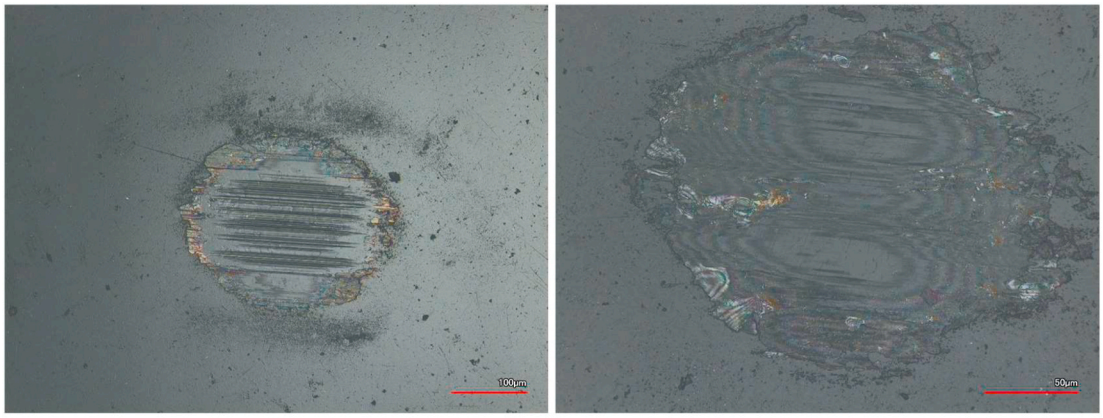

Fig. 5. Confocal and 3D images of the contact area of the alumina balls rubbed against the (a) Au and (b) Au-0.48SiO2 coatings after the 20.000 cycles at 2 Hz and 2.8 N.

4. Discussion

4.1. Frictional behaviour of gold and gold composite coatings

The tribological system under study consists in an alumina ball sliding against a Ni substrate coated with Au or Au–SiO_2 composites. According to the classical approach by Bowden and Tabor [19] two friction contributing components should be considered: the component μ_{adh} due to adhesion between the alumina and the gold (or nickel at a later stage of the experiments) and the ploughing term μ_{def} (see equation (1))

$$\mu = \mu_{adh} + \mu_{def} \quad (1)$$

The ploughing term can be estimated by assuming a perfectly plastic behaviour of gold. The area of the indent created by pressing the hard ball onto the soft gold coatings corresponds to the ratio between applied normal load and hardness of the coating. In the case of an applied normal load of 5 N and the hardness of 1060 MPa (hardness of the gold coating) one obtains a contact area of 0.0048 mm^2. The spherical cap geometry of the indent can be approximated to a circle because the indentation depth is much smaller than the radius (R) of the indenting ball. Therefore, the radius (r) of the contact area corresponds to the square root of that contact area divided by π and is 0.039 mm. The ball indentation defines a circular segment of base radius of r. The circular segment included angle θ and the segment area (S) can be obtained by the mensuration formulas given in equations (2) and (3) respectively:

$$r = R \sin \theta/2 \quad (2)$$

$$S = 0.5\ R^2\ (\theta - \sin \theta) \quad (3)$$

Introducing in equations (2) and (3) the values of 0.039 mm and 3 mm for r and R respectively, one obtains a segment area of 1.3 10^{-5} mm^2. The ploughing component μ_{def} is obtained by multiplying this segment area by the hardness of the metal and dividing it by the normal force. In this way one yields a maximum value for μ_{def} of less than 0.003. Thus, one can conclude that friction is essentially determined by the adhesive component.

The adhesive term of friction can be calculated using the asperity junction model described by equation 4

$$\mu_{adh} = \frac{1}{2\left[(\tau_c/\tau_i)^2 - 1\right]^{0.5}} \quad (4)$$

where τ_c is shear strength of the material (i.e. the coating) and τ_i is shear strength of the alumina/coating interface. The shear strength of the material τ_c can be calculated by assuming that the indentation hardness is about three times the uniaxial yield strength of the material and that the yield stress is around 2 times the yield stress in pure shear. In the case of the gold coating laded at 2.8 N the hardness is 1060 MPa (i.e. $\tau_c = 177$ MPa) and the COF measured at the onset of the rubbing before the raise due to the exposure of Ni is approximatively 0.25. Inserting these values in equation (2) yields $\tau_i = 80$ MPa. By combining this τ_i value (we assume that the small amount of incorporated SiO_2 particle does not affect significantly the interfacial properties) with the hardness values of the Au–SiO_2 coatings, one obtains, using equation (2), values for μ_{adh} of 0.20 and 0.18 for the Au-0.48SiO2 and Au-2.4SiO2, respectively. These values correspond indeed very well with the experimental ones listed in Table 2. Interestingly, the literature reported adhesive strength between alumina and gold in the order of 1–50 MPa depending on measurement method and metallurgical state of gold [20]. The value determined here of 80 MPa fits reasonably well these experimental results from literature. Note that equation (2) predicts that friction is independent on normal load. This is again in agreement with the present results (Table 2).

Noteworthy is that the present results indicate a decrease of the COF values at higher frequency, i. e higher sliding velocities. It has been reported that the hardness of gold increases with the indentation strain rate [21] and thus its shear strength also increases with strain rate. According to equation (2) this should result in a reduction of friction at higher frequency as indeed experimentally observed. Note however that the literature values on strain rate dependence of gold hardness were obtained at relatively slow strain rates and thus they do not necessarily represent the situation encountered in the present tribological contacts. Thermal effects seem to play a secondary role here. Indeed, the strength of gold was found to decrease with increasing temperature [22] while the interfacial strength with alumina was found to increase [23]. This should lead, according to equation (2), to higher friction, i.e. the opposite effect as observed here (Table 2).

4.2. Degradation mechanisms of gold and gold composite coatings on nickel

The post mortem analysis of the wear tracks revealed specific features including: surface smearing, subsurface deformation with local exposure of substrate nickel, and the third body layer constituted by a mixed nickel and aluminium oxide with some local mixing with metallic gold. The appearance of such features can be explained by the following sequence of events and illustrated in Fig. 9.

First, plastic deformation (Fig. 9b) and ploughing of the Au coating

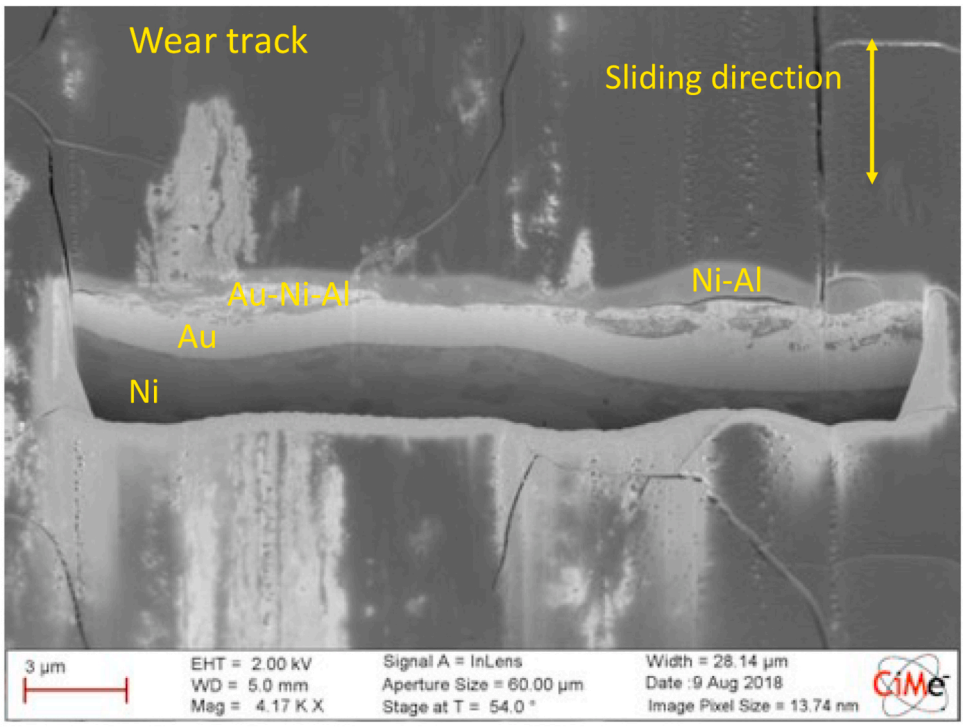

(a)

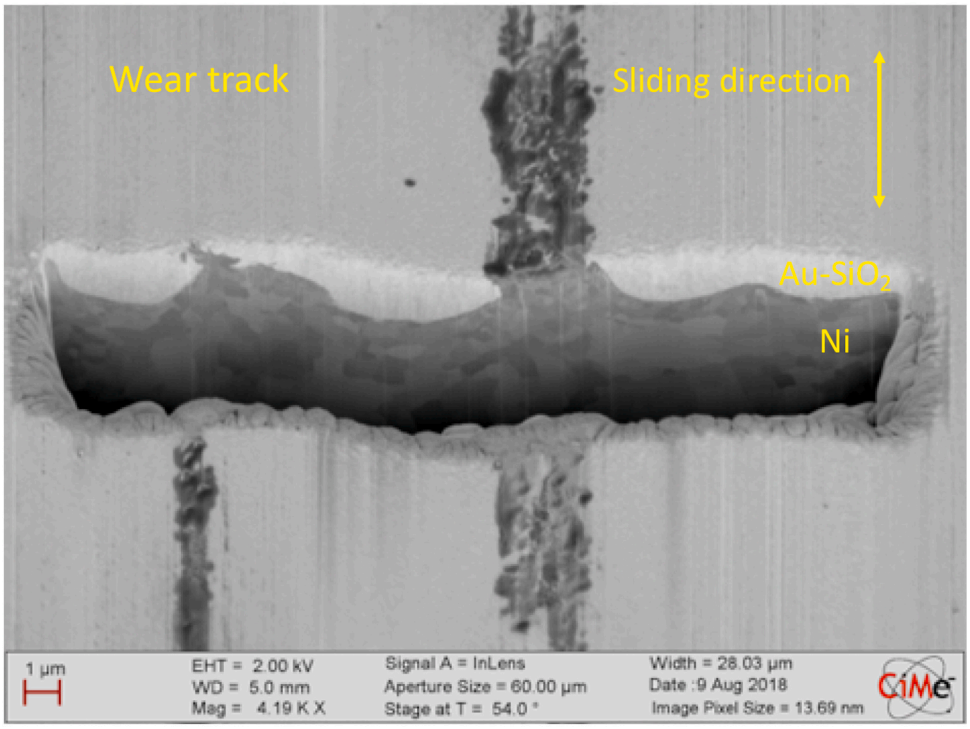

(b)

Fig. 6. FIB cross section of the (a) Au and (b) Au-0.48SiO2 composite coating after sliding 20.000 cycles against an alumina counterpart at 2 Hz and 2.8 N.

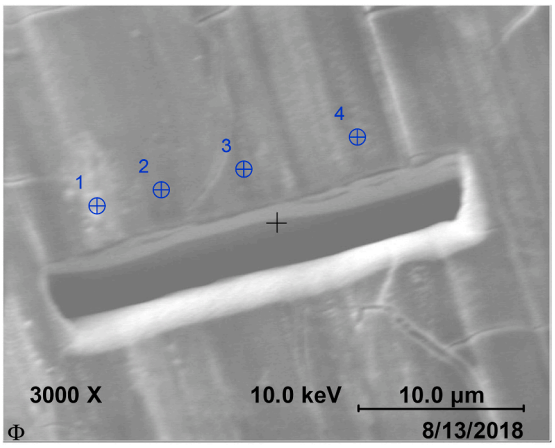

(a) SEM image

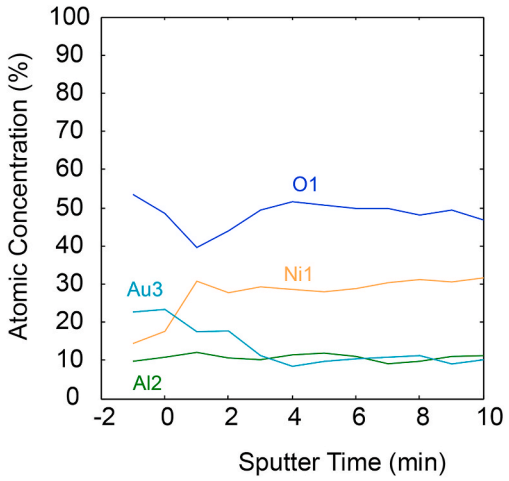

(b) AES profile point 1

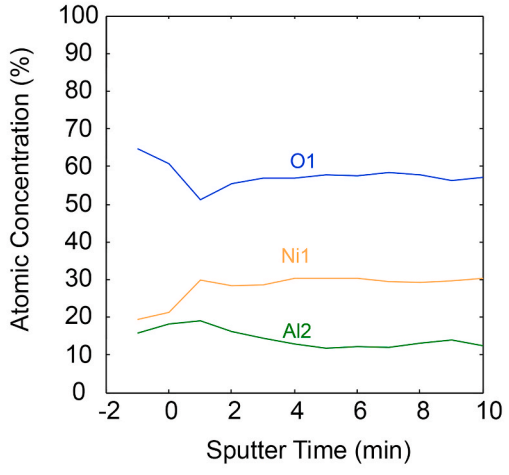

(c) AES profile point 2

Fig. 7. (a) SEM image of the FIB cross-section carried out in the wear track of the Au-coating with the numbers indicating the specific points in which AES profiles were carried out. (b) AES profiles with the atomic concentration of the different elements as a function of sputter time in position 1 and (c) in position 2.

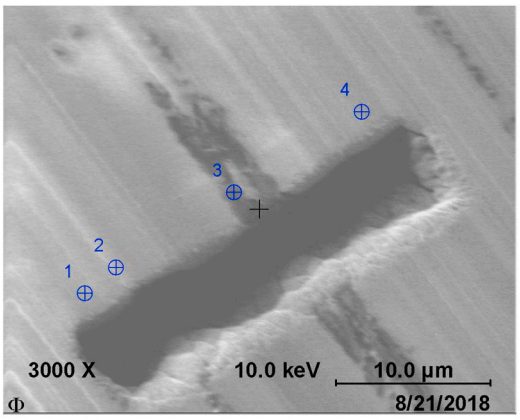

(a) SEM image

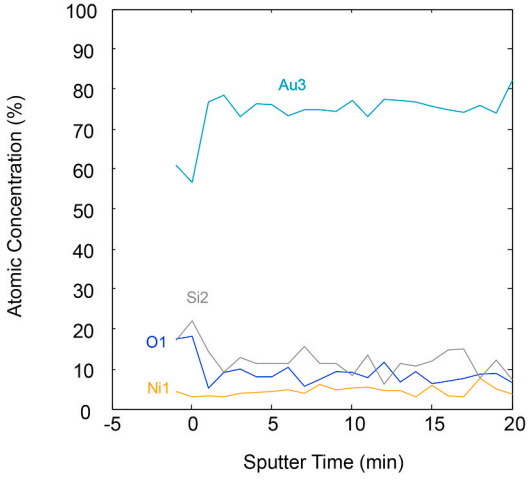

(b) AES profile point 1

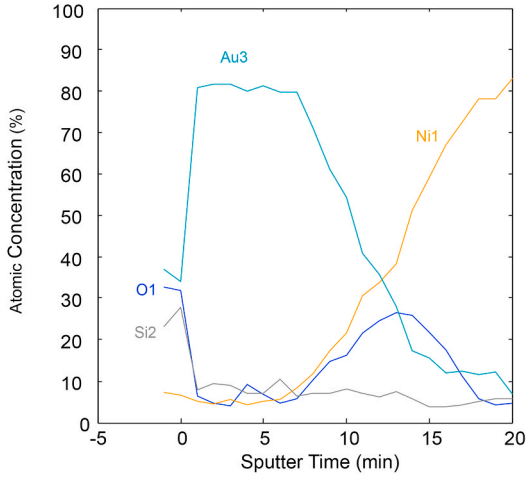

(c) AES profile point 3

Fig. 8. (a) SEM image of the FIB cross-section carried out in the wear track of the Au-0.48SiO2 coating with the numbers indicating the specific points in which AES profiles were carried out. (b) AES profiles with the atomic concentration of the different elements as a function of sputter time in position 1 and (c) in position 3.

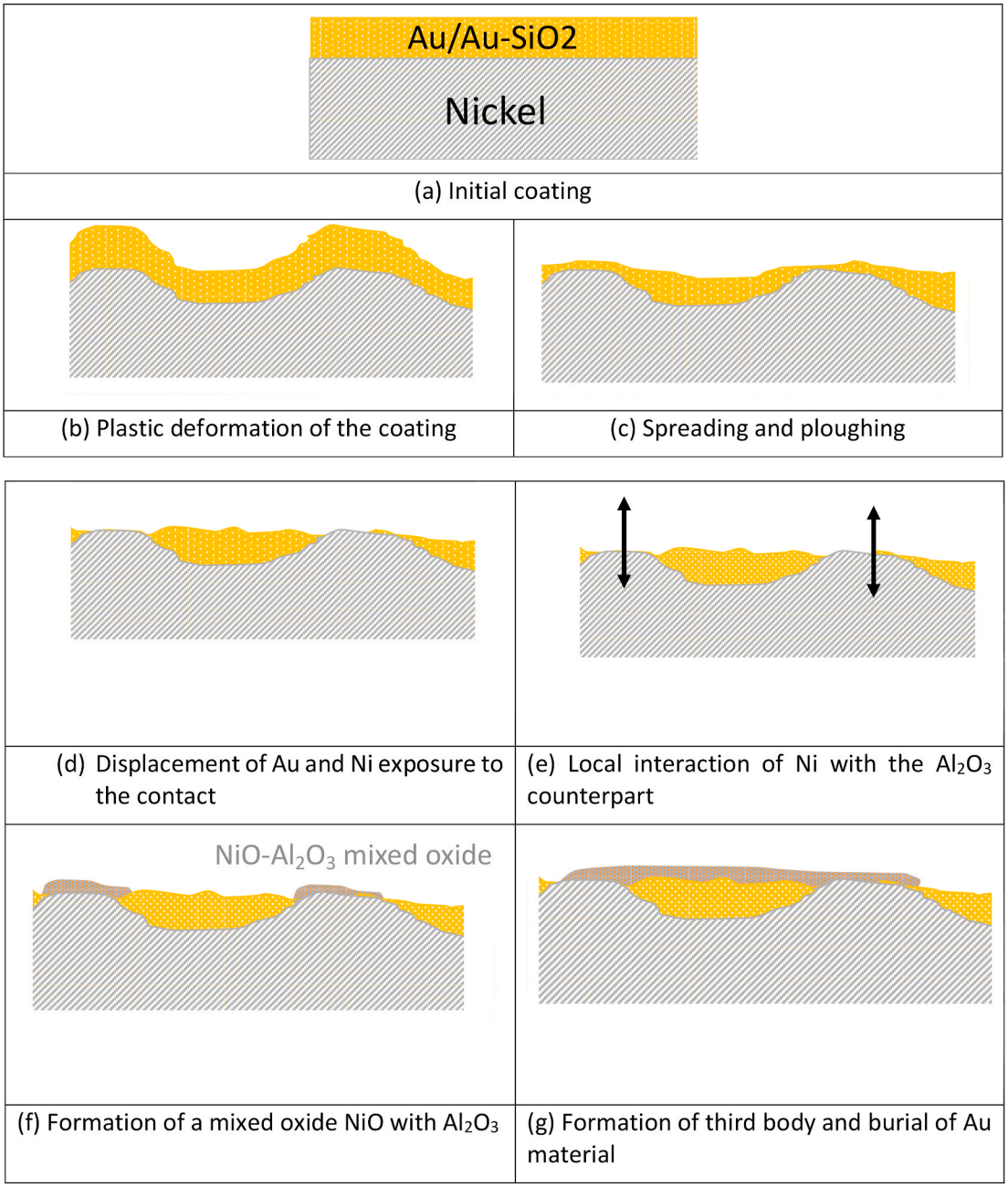

Fig. 9. Scheme of the different steps describing the wear mechanisms of Au and Au–SiO_2 composite coatings on a Ni substrate.

and Ni substrate occur with the subsequent smearing of the gold material along the wear track (Fig. 9c). The accumulation of plastic deformation in the gold due to the cyclic loading results in a final tear of the coating within the subsequent localized contact of the nickel substrate with the alumina counterpart (Fig. 9d). At this stage, the strong adhesion between this metal and alumina increases friction, promotes pulling off of nickel from the subsurface and its chemical interaction with alumina (Fig. 9e). Despite its hardness, alumina sliding against nickel is known to undergo wear through the formation of mixed NiO–Al_2O_3 oxides [24] (Fig. 9f). Indeed, the AES profiles show the build-up of this mixed oxide layer (Fig. 7). Locally, this layer can mix with smeared gold and get cracked (Fig. 9g). Interestingly, this sequence is observed in the case of the pure gold coating. In presence of silica only surface smearing of the coatings is observed with isolated upsurge of nickel. No mixed oxide layer can be observed (Fig. 8). This suggests that the higher hardness of the composite coatings delays the first nickel-alumina contacts and thus the mixing of alumina and nickel oxide and the formation of the third body. Indeed, the exposure of Ni to the contact in presence of SiO_2 nanoparticles in the Au coating was only observed locally after the 20.000 cycles of the tribological tests.

4.3. Wear of gold and gold composite coatings on nickel

The presence of small amounts of transferred gold on the alumina ball (Fig. 5) is an evidence for wear of the gold coating. In order to quantify the amount of wear, five 2D cross section profiles were extracted from the profilometry images shown in Fig. 3. After subtraction of the base line, defined by the flat regions outside of the wear tracks not modified by the ridges, the average depth of the region inside of the wear track was determined. For the Au coating we obtain an average wear track depth of 38 nm while for the Au-0.48 SiO2 and Au-2.4 SiO2 the average depths are −35 nm and −25 nm, respectively.

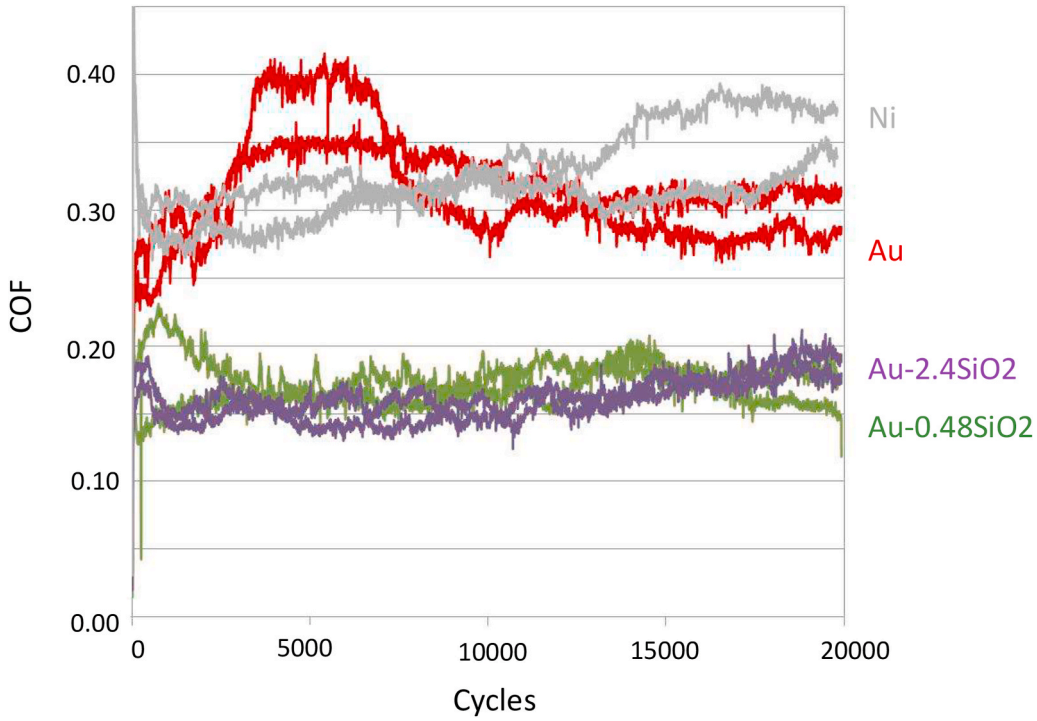

Fig. 2. Typical evolution of the coefficient of friction of Ni, Au and Au–SiO_2 composite coatings sliding against an alumina ball at 2 Hz and 2.8 N.

This shows that gold removal by wear from the composite coatings is very limited and corresponds (considering the wear track width and length of 0.2 and 3 mm, respectively) to a low wear rate in the range of 10^{-8} to 10^{-7} mm^3/Nm. The FIB cross sections confirm the low wear as they show that the gold layer was deformed but its average thickness was little altered.

The positive value in the case of the Au coating is due to the build-up of the mixed Ni–Al oxide layer. Interestingly, the thickness of this third body layer is approximately 500–1000 nm (FIB cross section in Fig. 6). Interestingly, also in Fig. 6a the thickness of the gold layer seems unaltered with respect to the initial one (Fig. 1b). This indicates that the gold layer was displaced below the original surface by the upsurge of nickel and its reaction with alumina. Clearly, the main function of the SiO_2 particles is to postpone the nickel substrate exposure to the contact and the associated formation of third body that at the end buries the gold layer.

5. Conclusions

The main outcomes of the obtained results lead to the following conclusions:

- Composite gold coatings containing SiO_2 nanoparticles could be produced by galvanostatic electrochemical deposition from a colloidal suspension. These composite coatings exhibit higher hardness than the gold coating while all coatings showed very similar roughness and elastic properties.
- The composite coatings exhibit lower coefficient of friction. This is because friction, in the studied tribological configuration, is controlled by the adhesive component that is inversely proportional to hardness.
- The friction reducing effect of the gold coating was found limited by the exposure of the nickel substrate as a consequence of subsurface deformation and gold smearing. The composite coatings by exhibiting higher hardness and reducing friction, delay the exposure of nickel.
- The incorporation of SiO_2 nanoparticles into the gold matrix prolongs the solid lubricant effect of the coating by a factor of 10.
- No significant wear of the gold composite layers was observed.

Declaration of competing interest

The authors declare that they have no known competing financial interests or personal relationships that could have appeared to influence the work reported in this paper.

Acknowledgements

This research has been financially supported by the Swiss Innovation Agency-Innosuisse within the frame of the CTI project18738.1 PFNM-NM.

References

[1] M. Antler, Electrical effects of fretting connector contact materials: a review, Wear 106 (1985) 5–33.
[2] M. Antler, Survey of contact fretting in electrical connectors, LEEE Trans. Companents Hybkis Manuf. Tech. 8 (1) (1985) 87–104.
[3] Modern Electroplating Edited by Mordechay Schlesinger and Milan Paunovic, John Wiley, 2010.
[4] M. Antler, Tribology of metal coatings for electrical contacts, Thin Solid Films 84 (1981) 245–256.
[5] Y. Okinaka, M. Hoshino, Some recent topics in gold plating for electronics applications, Gold Bull. 31 (1998) 3–13.
[6] Y. Miyakawa, Friction and wear performance of gold and gold alloy films, Gold Bull. 13 (1980) 21–30.
[7] T. Spalvins, A review of recent advances in solid film lubrication, J. Vac. Sci. Technol., A 5 (1987) 212–219.
[8] H. Tian, N. Saka, E. Rabinowicz, Fretting failure of electroplated gold contacts Wear 142 (1991) 265–289.
[9] R.G. Bayer, E. Hsue, J. Turner, A motion-induced sub-surface deformation wear mechanism, Wear 154 (1992) 193–204.
[10] V. Magnin, S. Mischler, Tribological response of multilayered gold nickel coating deposited on fine turned surfaces, Wear 426–427 (2019) 1195–1202.
[11] P.A. Engel, E.Y. Hsue, R.G. Bayer, Hardness, friction and wear of multiplated electrical contacts, Wear 162–164 (1993), 538-531.
[12] A.R. Shugurov, A.V. Panin, A.O. Lyazgin, E.V. Shesterikov, Wear of electroplated gold-based coatings Physical Mesomechanics 19 (2016) 407–419.

[13] A.K. Chaudhari, V.B. Singh, A review of fundamental aspects, characterization and applications of electrodeposited nanocrystalline iron group metals, Ni-Fe alloy and oxide ceramics reinforced nanocomposite coatings, J. Alloys Compd. 751 (2018) 194–214.
[14] F.C. Walsh, C. Ponce de Leon, A review of the electrodeposition of metal matrix composite coatings by inclusion of particles in a metal layer: an established and diversifying technology, Trans. Inst. Met. Finish. 92 (2014) 83–98.
[15] D.K. Singh, V.B. Singh, Electrodeposition and characterization of Ni-TiC composite using N-methylformamide bath, Mater. Sci. Eng. 532 (2012) 493.
[16] S.T. Aruna, V.K.W. Grips, K.S. Rajam, Ni-based electrodeposited composite coating exhibiting improved microhardness, corrosion and wear resistance properties, J. Alloys Compd. 468 (2009) 546.
[17] J. Song, K.C. Koch, L. Wang, Correlation between wear resistance and lifetime of electrical contacts, Adv. Tribol. (2012) 1–9, 2012.
[18] D. Erogluz, A.C. West, Mathematical modeling of Ni/SiC Co-deposition in the presence of a cationic dispersant, J. Electrochem. Soc. 160 (2013) D354.
[19] F.P. Bowden, D. Tabor, The Friction and Lubrication of Solids Part I, The Clarendon Press, oxford, 1986.
[20] A.J. Pedraza, R.A. Kumar, D.H. Lowndes, Greatly improved adhesion of gold films sputter-deposited on laser-tretaed and thermally annealed alumina, Appl. Phys. Lett. 66 (1995) 1065.
[21] L. Wang, B.C. Prorok, Characterization of the strain rate dependent behavior of nanocrystalline gold films, J. Mater. Res. 23 (2008) 55–65.
[22] D.S. Liu, Y.C. Chao, Effects of dopant, temperature, and strain rate on the mechanical properties of micrometer gold-bonding wire, J. Electron. Mater. 32 (2003) 159–165.
[23] A. Assaban, M. Gillet, Adhesion of gold and copper thin films deposited on alumina and magnesium oxide, J. Adhes. Sci. Technol. 13 (1999) 871–885.
[24] J. Du, S. Cao, A. Igual Munoz, S. Mischler, Tribological and Tribocorrosion Behavior of Nickel Sliding against Oxide Ceramics Wear, vol. 426–vol. 427, 2019, pp. 1496–1506.